NANO LETTERS

pubs.acs.org/NanoLett Letter

Magneto-Optical Sensing of the Pressure Driven Magnetic Ground States in Bulk CrSBr

Amit Pawbake,* Thomas Pelini, Ivan Mohelsky, Dipankar Jana, Ivan Breslavetz, Chang-Woo Cho, Milan Orlita, Marek Potemski, Marie-Aude Measson, Nathan P. Wilson, Kseniia Mosina, Aljoscha Soll, Zdenek Sofer, Benjamin A. Piot, Mike E. Zhitomirsky, and Clement Faugeras*

Cite This: *Nano Lett.* 2023, 23, 9587−9593 Read Online

ACCESS | Metrics & More | Article Recommendations | Supporting Information

ABSTRACT: Competition between exchange interactions and magnetocrystalline anisotropy may bring new magnetic states that are of great current interest. An applied hydrostatic pressure can further be used to tune their balance. In this work, we investigate the magnetization process of a biaxial antiferromagnet in an external magnetic field applied along the easy axis. We find that the single metamagnetic transition of the Ising type observed in this material under ambient pressure transforms under hydrostatic pressure into two transitions, a first-order spin-flop transition followed by a second-order transition toward a polarized ferromagnetic state near saturation. This reversible tuning into a new magnetic phase is obtained in layered bulk CrSBr at low temperature by varying the interlayer distance using high hydrostatic pressure, which efficiently acts on the interlayer magnetic exchange and is probed by magneto-optical spectroscopy.

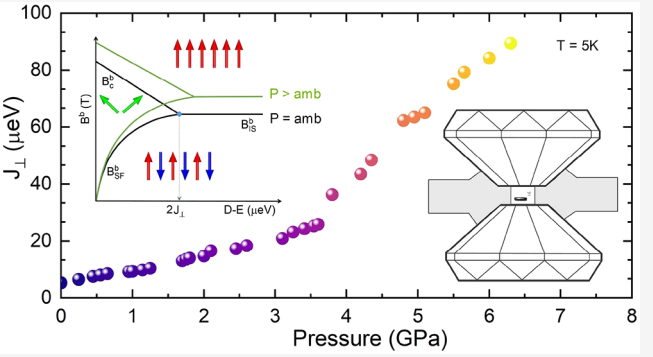

KEYWORDS: *van der Waals materials, magnetic materials, extreme conditions, optical spectroscopy, magnetic phase transition*

Downloaded via CNRS REGION RHONE ALPES on October 29, 2023 at 10:23:38 (UTC).
See https://pubs.acs.org/sharingguidelines for options on how to legitimately share published articles.

The generation of new magnetic phases by an external manipulation of the magnetic state is a requirement for the implementation of new spintronic and magnontronic functionalities. Successful manipulations of magnetic states have been achieved by using spin-polarized electrical currents,[1] electrostatic gating,[2] or ultrafast laser excitations.[3,4] An alternative approach relies on the direct modification of the magnetic interactions by changing the lattice parameters and/or the superexchange paths by applying strain[5] or hydrostatic pressure.[6,7] Such profound modifications affect both direct-exchange magnetic interaction and spin−orbit interaction-related effects, such as magnetocrystalline anisotropy, which determines the preferential directions of spins in a magnetically ordered solid and the spin wave energy.

Magnetic van der Waals (vdW) materials are layered crystals with magnetic properties that can be thinned down to the monolayer limit. They exhibit a broad variety of ordered magnetic structures.[8,9] Recently, vdW magnets have attracted a lot of interest and stimulated many experimental and theoretical studies aiming at understanding their magnetic properties and at using them within functional vdW heterostructures.[10,11] The observation of long-range magnetic order in the 2D limit[12,13] that is precluded by the Mermin−Wagner theorem[14] is understood as a consequence of substantial magnetocrystalline anisotropy and of the associated energy gap in the spin wave dispersion.[15] vdW materials offer new, exciting possibilities to engineer magnetic properties of solid-state systems because they are characterized by a very strong structural anisotropy: individual layers are bound together by weak vdW interactions. As a result, the interlayer spacing, the vdW gap, can be tuned efficiently through the application of hydrostatic pressure.[6,7,16,17] Such changes strongly affect the short-range interlayer interactions[18,19] and the competition between magnetic exchange interactions and magnetic anisotropies. New magnetic phases can be engineered in a magnetic system by changing the competition between the anisotropies and exchange interactions.

In this article, we apply hydrostatic pressure to bulk CrSBr to tune the interlayer magnetic exchange interaction and the magnetocrystalline anisotropies. We sense the induced changes by magneto-photoluminescence measurements with an external magnetic field applied along one of the three crystallographic axis. The interlayer exchange parameter $J_\perp$ responsible for the antiferromagnetic (AFM) ordering is small

Received: August 26, 2023
Revised: October 6, 2023
Published: October 12, 2023

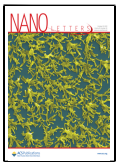

ACS Publications © 2023 American Chemical Society

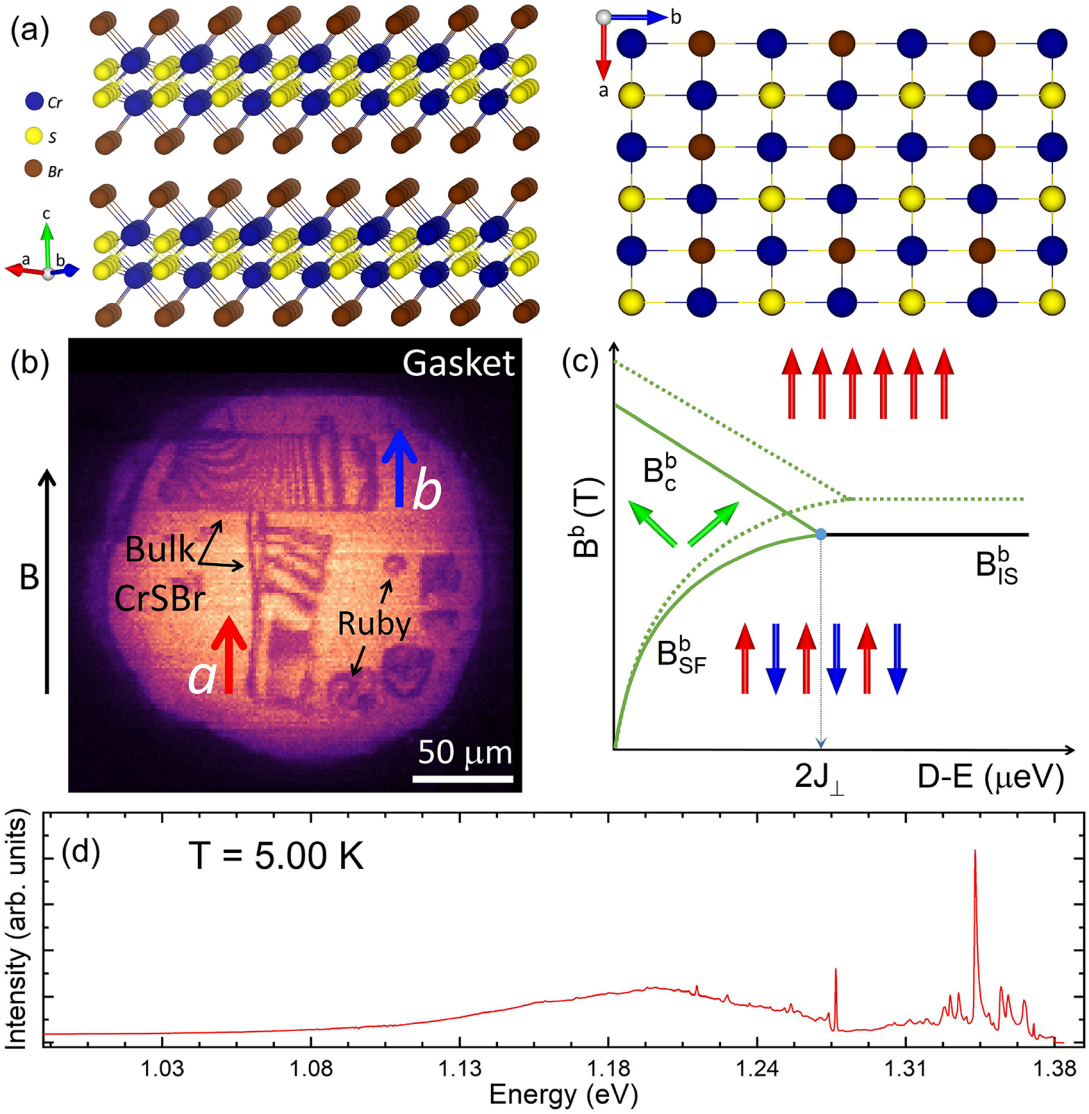

Figure 1. (a) Crystallographic structure of bulk CrSBr. (b) Optical image of the pressure chamber of the diamond anvil cell showing two pieces of CrSBr with different orientations and ruby balls. (c) (Solid lines) Schematics of the magnetic phase diagram of easy-plane AFM for a fixed value of $J_\perp$ showing the antiferromagnetic, the ferromagnetic, and the spin-flop magnetic phases. The spin-flop phase appears when the anisotropy difference (D,E) becomes smaller than the interlayer exchange $J_\perp$. We indicate the critical values of the magnetic field for spin-flip B^b_c, for the abrupt Ising transition B^b_{IS} and for the spin-flop B^b_{SF}. The dashed lines represent a similar phase diagram with a higher value of $J_\perp$. (d) Typical photoluminescence spectrum of bulk CrSBr at T = 5 K showing the excitonic lines around 1.35 eV and a broad emission at lower energies.

in bulk CrSBr because of its lamellar structure. When the vdW gap is decreased, we observe an increase of $J_\perp$ by 1700% at $P >$ 6 GPa. This large increase with respect to magnetocrystalline anisotropies stabilizes CrSBr into a particular magnetic ground state characterized by an intermediate spin-flop phase appearing between the AFM ground state at B = 0 and the ferromagnetic (FM) ground state when an external magnetic field, exceeding the saturation field, is applied (see Figure 1c). This new magnetic ground state is observed because of the possibility to tune the competition between the interlayer exchange interaction and the magnetocrystalline anisotropies without changing the crystallographic stacking. When the hydrostatic pressure is further increased, the in-plane magnetocrystalline anisotropy vanishes, thereby transforming CrSBr into an easy-axis AFM.

CrSBr is an air-insensitive layered direct band gap semiconductor with E_g = 1.5 eV hosting tightly bound excitons that give rise to photoluminescence signals close to 1.35 eV[20] at low temperature. It crystallizes in the P*mmn* space group in an orthorhombic structure in which monolayers are bound together by vdW interactions, see Figure 1a. From the point of view of magnetism, CrSBr belongs to the class of easy-axis layered AFM systems with an in-plane anisotropy. Below the Curie temperature of T_C = 160 K, magnetic moments in the layers orient ferromagnetically along the easy axis,[21] the crystallographic **b** axis. Below the Néel temperature of T_N = 132 K, an AFM interaction couples each layer. Below T = 40 K, various experimental signatures of a change in the magnetic ground state have been reported,[20,22−25] even though the low-temperature magnetic behavior is the one of a layered antiferromagnet.[26] This low-temperature behavior was recently attributed to the ferromagnetic ordering of defects.[27] When magnetically ordered, bulk CrSBr is an ensemble of anisotropic FM planes with an AFM coupling of adjacent planes.[28] In multilayer CrSBr, the interlayer hopping is spin-dependent, which makes the energy of electronic states different for an

https://doi.org/10.1021/acs.nanolett.3c03216
Nano Lett. 2023, 23, 9587−9593

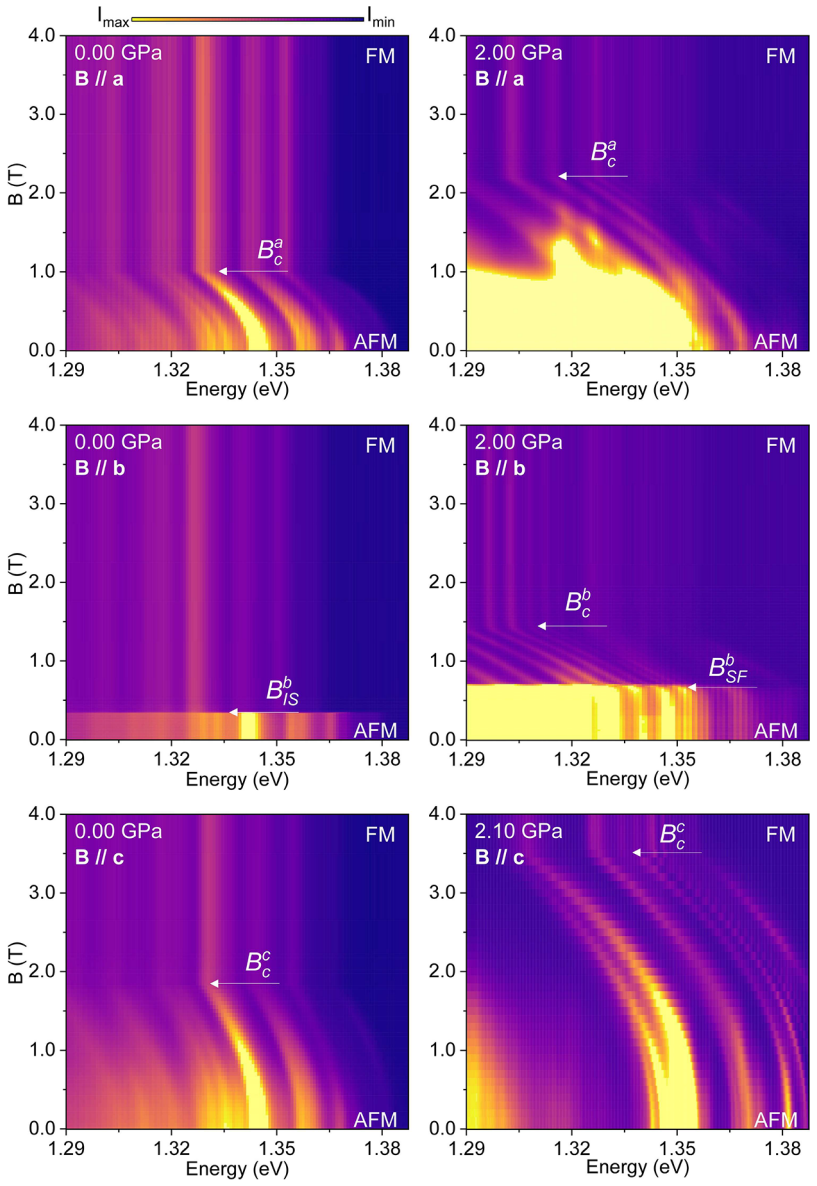

Figure 2. False color maps of the low-temperature magneto-photoluminescence response of bulk CrSBr for the different values of hydrostatic pressure when the magnetic field is applied along the *a* axis (top row), the *b* axis (middle row), and the *c* axis (bottom row). The white arrows indicate the critical magnetic fields.

AFM or FM ground state.[26] This energy difference can be seen in the emission energy of the exciton, which can then be used to determine, for instance, the value of saturation of magnetic fields and to characterize the magnetic ground state.[5] The electronic properties of CrSBr are strongly anisotropic, and this is reflected in its optical[26,29] and transport properties.[30] Low-energy excitations in CrSBr include two magnon excitations at 25 and 35 GHz.[31−33] CrSBr exhibits two inequivalent magnetic ions in the magnetic unit cell and, hence, a higher-energy magnon branch.[31] Our infrared magneto-transmission experiments presented in Figure S1 of the Supporting Information, show an absorption at 372 cm^{-1} that disperses linearly with the external magnetic field with a *g*-factor close to 2, which we identify as the second magnon branch of bulk CrSBr.

To measure the low-temperature magneto-optical properties of bulk CrSBr under hydrostatic pressure, we use the experimental setup described in ref 34. A diamond anvil cell (DAC) is placed on piezo motors to allow for its displacement under the excitation laser spot produced by a long working distance objective. The pressure value at low temperature is determined by the photoluminescence of the ruby balls. Bulk CrSBr was grown by chemical vapor transport (Supporting Information). Crystals with typical sizes of a few tens of micrometers were inserted in the pressure chamber of the DAC, as shown in Figure 1b, and could be oriented by taking advantage of the strong shape anisotropy of this material that produces crystals elongated along the *a* crystallographic axis (see Figure 1b). The DAC can be oriented at room temperature to apply the external magnetic field along different crystal directions (see Figure S2 of the Supporting Information). This allows for comparison of the pressure-dependent magneto-optical response, which gives access to the parameters describing the magnetic Hamiltonian. All measurements presented in this work have been performed at a temperature of $T = 5$ K. Each value of the hydrostatic pressure

https://doi.org/10.1021/acs.nanolett.3c03216
Nano Lett. 2023, 23, 9587−9593

was first applied at room temperature, and the DAC was then cooled for optical spectroscopy measurements.

A typical low-temperature photoluminescence spectrum of bulk CrSBr is presented in Figure 1d. It includes an ensemble of sharp emission lines around 1.35 eV related to excitons and exciton−polaritons,[26,35] while lower energy broad emissions are related to defects.[24]

We present in Figure 2 false color maps of the evolution of the low-temperature photoluminescence spectrum of CrSBr at ambient pressure and at $P \approx 2$ GPa with the magnetic field applied along the a (top row), b (middle row), and c axis (bottom row). When the magnetic field is applied along the intermediate a or the hard c axis, the two spin sublattices gradually cant toward the direction of the external field. The exciton energy slowly evolves from the $B = 0$ energy to a lower-energy representative of the band structure of CrSBr with a FM magnetic ordering.[26] When hydrostatic pressure is applied, we observe a pronounced increase of the saturation magnetic fields B_c^a and B_c^c (B_c^α is the critical magnetic field when the external magnetic field is applied along the a axis), which indicates a change in the competition between magnetic exchange and magnetocrystalline anisotropy. The complete evolution is presented in Figures S3−S5 of the Supporting Information. If the external B field is applied along the b axis, then the observed behavior is different. At ambient pressure, the AFM to FM transition is abrupt (Ising transition or strong anisotropy regime) at saturation field B_{IS}^b. When a hydrostatic pressure above $P = 1$ GPa is applied, we observe a different behavior: the exciton energy remains constant up to a saturation field B_{SF}^b above which it initiates an approximately linear red shift up to a second value of the magnetic field labeled B_c^b. For $B > B_c^b$, the exciton emission energy remains constant, thereby indicating that CrSBr is in a FM ground state. The intermediate behavior observed when $B_{SF}^b < B < B_c^b$ appears as a gradual decrease of the emission energy when the magnetic field is increased. This behavior is similar to that observed when the external magnetic field is applied along the a or c axis and describes the gradual canting of the spins toward the direction of the applied magnetic field.

To understand these results, we use the following microscopic spin Hamiltonian, which is suitable for describing the two-sublattice orthorhombic AFM CrSBr:

$$\hat{\mathcal{H}} = \sum_{\langle ij \rangle} J_{ij} \mathbf{S}_i \times \mathbf{S}_j + \sum_i \{-D(S_i^b)^2 + E[(S_i^c)^2 - (S_i^a)^2] - g_\alpha \mu_B B^\alpha S_i^\alpha\} \quad (1)$$

Here, $\mathbf{S}_i$ is $S = 3/2$ spins of chromium ions, J_{ij} is the exchange coupling constant, and D and E are parameters of biaxial single-ion anisotropy with α being either b (easy axis) or a [intermediate axis $(D > E)$], and c is the hard axis. Stable magnetic configurations can be determined by treating spins as classical vectors and minimizing the corresponding energy (eq 1). In this way, one can find that FM exchanges inside the ab layers play no role in the magnetization process, which depends only on the AFM interlayer coupling $J_\perp > 0$. The three nearest neighbors exchange integrals have been determined by neutron scattering, and their values are found to be 2 orders of magnitude larger than the interlayer one,[36] so spins within the layers remain parallel to each other to minimize the intralayer exchange energy.

Magnetic field applied perpendicular to the easy-axis causes continuous spin tilting in the canted AFM state (CAF) until the full saturation is reached at the critical (second-order) field

$$g_a \mu_B B_c^a = 2S(4J_\perp + D - E) \quad (2)$$

$$g_c \mu_B B_c^c = 2S(4J_\perp + D + E) \quad (3)$$

where g_α is the g-factor when the external magnetic field is applied along the α axis.

Once an external field is applied along the easy axis of a collinear AFM, the magnetization remains zero until the spin-flop transition. The corresponding expression for the spin model of CrSBr

$$g_b \mu_B B_{SF}^b = 2S\sqrt{(D - E)(4J_\perp - D + E)} \quad (4)$$

Above B_{SF}^b, the AFM sublattices rotate abruptly toward the intermediate a axis to form the CAF state. The full saturation is reached at

$$g_b \mu_B B_c^b = 2S(4J_\perp - D + E) \quad (5)$$

Thus, the conventional magnetization process for a collinear AFM proceeds as $\uparrow\downarrow \rightarrow$ CAF $\rightarrow \uparrow\uparrow$.

The above picture suggested by Louis Néel[37] needs to be modified for CrSBr. Because of a large $D/J_\perp$, this AFM undergoes a direct first-order transition from the collinear AFM state into the fully polarized state typical for magnets with strong Ising anisotropy

$$g_b \mu_B B_{IS}^b = 4J_\perp S \quad (6)$$

The Ising-like transition for $B \| b$ has been experimentally observed in CrSBr.[26,33,38] It corresponds to an abrupt reversal of magnetization in every second Cr layer. We find by comparing eqs 4−6 that the conventional magnetization process is realized for $(D - E) < 2J_\perp$, whereas for $(D - E) > 2J_\perp$, the direct transition $\uparrow\downarrow \rightarrow \uparrow\uparrow$ takes place. The corresponding $T = 0$ phase diagram is sketched in Figure 1c.

Our main experimental observation is the tuning of bulk CrSBr from the strong to the weak anisotropy regime for which a spin-flop phase is stabilized. Crossing this boundary is a unique possibility offered by bulk CrSBr for which $(D - E)$ and $2J_\perp$ are comparable at ambient pressure. The tuning is achieved by applying hydrostatic pressure, which strongly enhances the interlayer coupling $J_\perp$ such that $(D - E)/2J_\perp$ becomes smaller. For $P > 4$ GPa, the measured saturation field B_c^b along the b axis increases and becomes almost equal to the one along the a axis. This evolution describes a decrease of the in-plane anisotropy $[(D - E) \rightarrow 0]$ such that the (a, b) plane becomes nearly isotropic.

Specifically, Figure 3a shows the evolution of the measured values of the saturation magnetic fields along the three crystallographic axis. They strongly increase with the applied hydrostatic pressure, and at each pressure value we can determine from eq 2−6 the three microscopic parameters $J_\perp$, D, and E. The evolution with pressure of these parameters is presented in Figure 3b. At ambient pressure, we find that $J_\perp = 5.3$ μeV, $D = 33.0$ μeV, and $E = 16.36$ μeV, which is in line with recent GHz investigations conducted on bulk material from the same batch.[33] At ambient pressure, bulk CrSBr is in the strong anisotropy regime fulfilling the condition $(D - E) > 2J_\perp$. When hydrostatic pressure is applied, the lattice parameters and, in particular, the vdW gap are changed, and

https://doi.org/10.1021/acs.nanolett.3c03216
Nano Lett. 2023, 23, 9587−9593

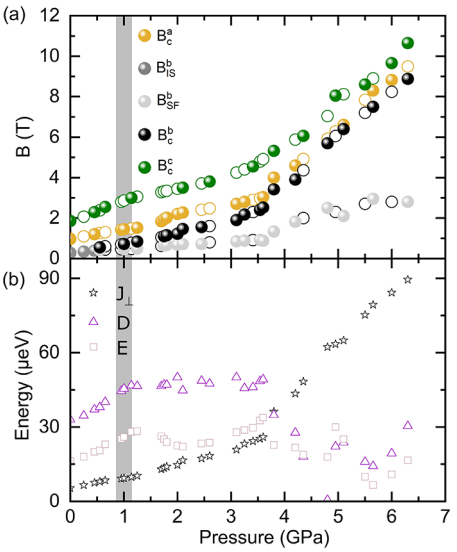

Figure 3. (a) Critical magnetic fields along the hard c axis (green symbols), the intermediate a axis (orange symbols), and along the easy b axis (black symbols). Open symbols are extrapolated from nearby measurements. (b) Evolution of the microscopic parameters describing the interlayer interaction $J_\perp$, the easy-axis anisotropy D, and the in-plane anisotropy E as a function of the applied pressure. The spin-flop phase is observed when $B^b_{SF} < B < B^b_c$. The gray region indicates the range of pressure for which $2J_\perp \approx (D - E)$.

both the magnetic anisotropies and the interlayer exchange interaction are modified, accordingly. $J_\perp$ is increased by 1700% at P = 6 GPa, in line with recent results obtained at lower pressure values.[39] Both D and E also increase significantly, but in a similar way, which keeps the difference $D - E$ at a constant value up to P = ∼3 GPa. The condition $(D - E) < 2J_\perp$, which is indicative of the weak anisotropy regime, is reached for $P \simeq$ 1 GPa. Above this pressure value, we observe the intermediate spin-flop phase when an external magnetic field is applied along the b axis and two saturation fields, as indicated in Figures 2 and 3. The range of magnetic field within which the spin-flop phase is observed increases with the applied pressure as the vdW gap shrinks and $J_\perp$ is increased. The variations of D or E are more likely related to deformations of the individual layers along the c axis (bond angles) and within the plane of the layers and also by a possible anisotropy of the Young's modulus.

Above P = 3.5 GPa, we note two main changes in the evolution of the microscopic parameters with pressure: Both D and E strongly decrease and become comparable, and the evolution rate of $J_\perp$ with the pressure increases significantly. These two points are the sign of change in the system, even though the observed behavior of the magneto-photoluminescence remains the same above and below this particular pressure value. As shown in Figure S6 of the Supporting Information, the application of hydrostatic pressure to bulk CrSBr is a reversible process.

To conclude, by applying high hydrostatic pressure to bulk CrSBr, we modified the competition between the crystalline magnetic anisotropy and the interlayer exchange parameter. On the basis of low-temperature magneto-photoluminescence measurements under such extreme experimental conditions, we have identified a spin-flop phase stabilized when the interlayer exchange interaction strongly exceeds the magnetic anisotropy. These results are understood in the frame of a spin Hamiltonian including magneto-crystalline anisotropies, which describes the appearance of the spin-flop magnetic phase when $(D - E) < 2J_\perp$ (weak anisotropy regime). Compared with the experimental results, this model provides values for the microscopic parameters entering the spin Hamiltonian, and their evolution can be traced up to P = 6 GPa. This work demonstrates the possibility of tailoring the competition between magnetic crystalline anisotropy and interlayer exchange interaction of vdW magnets by external means and enlarges the technical possibilities for the design of two-dimensional magnets.

■ ASSOCIATED CONTENT

Supporting Information

The Supporting Information is available free of charge at https://pubs.acs.org/doi/10.1021/acs.nanolett.3c03216.

Additional data and analysis, including details on experimental setup, sample preparation, and additional experimental data (PDF)

■ AUTHOR INFORMATION

Corresponding Authors

Amit Pawbake − *LNCMI, UPR 3228, CNRS, EMFL, Université Grenoble Alpes, 38000 Grenoble, France*; Email: amit.pawbake@lncmi.cnrs.fr

Clement Faugeras − *LNCMI, UPR 3228, CNRS, EMFL, Université Grenoble Alpes, 38000 Grenoble, France*; orcid.org/0000-0002-9615-8739; Email: clement.faugeras@lncmi.cnrs.fr

Authors

Thomas Pelini − *LNCMI, UPR 3228, CNRS, EMFL, Université Grenoble Alpes, 38000 Grenoble, France*

Ivan Mohelsky − *LNCMI, UPR 3228, CNRS, EMFL, Université Grenoble Alpes, 38000 Grenoble, France*

Dipankar Jana − *LNCMI, UPR 3228, CNRS, EMFL, Université Grenoble Alpes, 38000 Grenoble, France*

Ivan Breslavetz − *LNCMI, UPR 3228, CNRS, EMFL, Université Grenoble Alpes, 38000 Grenoble, France*

Chang-Woo Cho − *LNCMI, UPR 3228, CNRS, EMFL, Université Grenoble Alpes, 38000 Grenoble, France*

Milan Orlita − *LNCMI, UPR 3228, CNRS, EMFL, Université Grenoble Alpes, 38000 Grenoble, France*; orcid.org/0000-0002-9633-507X

Marek Potemski − *LNCMI, UPR 3228, CNRS, EMFL, Université Grenoble Alpes, 38000 Grenoble, France; CENTERA Laboratories, Institute of High Pressure Physics, PAS, 01−142 Warsaw, Poland*; orcid.org/0000-0001-8881-6618

Marie-Aude Measson − *Institut Neel, Université Grenoble Alpes, 38000 Grenoble, France*

Nathan P. Wilson − *Walter Schottky Institut, Physics Department and MCQST, Technische Universitat Munchen, 85748 Garching, Germany*

Kseniia Mosina − *Department of Inorganic Chemistry, University of Chemistry and Technology Prague, 166 28 Prague 6, Czech Republic*

Aljoscha Soll − *Department of Inorganic Chemistry, University of Chemistry and Technology Prague, 166 28 Prague 6, Czech Republic*; orcid.org/0000-0003-4797-0015

Zdenek Sofer − *Department of Inorganic Chemistry, University of Chemistry and Technology Prague, 166 28*

https://doi.org/10.1021/acs.nanolett.3c03216
Nano Lett. 2023, 23, 9587−9593

Prague 6, Czech Republic; orcid.org/0000-0002-1391-4448

Benjamin A. Piot − *LNCMI, UPR 3228, CNRS, EMFL, Université Grenoble Alpes, 38000 Grenoble, France;* orcid.org/0000-0003-4858-2452

Mike E. Zhitomirsky − *Université Grenoble Alpes, CEA, Grenoble INP, IRIG, Pheliqs, 38000 Grenoble, France; Institut Laue-Langevin, F-38042 Grenoble Cedex 9, France*

Complete contact information is available at: https://pubs.acs.org/10.1021/acs.nanolett.3c03216

Notes

The authors declare no competing financial interest.

■ ACKNOWLEDGMENTS

We thank Nicolas Ubrig and Gerard Martinez for valuable comments on the manuscript. This work has been partially supported by the EC Graphene Flagship project. M.E.Z. was supported by ANR Grant No. ANR-15-CE30-0004. M.-A.M. acknowledges the support from the ERC (H2020) (Grant agreement No. 865826). N.P.W. acknowledges support from the Deutsche Forschungsgemeinschaft (DFG, German Research Foundation) under Germany's Excellence Strategy—EXC-2111—390814868. We acknowledge the support of the LNCMI-EMFL, CNRS, Univ. Grenoble Alpes, INSA-T, UPS, Grenoble, France.

■ REFERENCES

(1) Katine, J. A.; Albert, F. J.; Buhrman, R. A.; Myers, E. B.; Ralph, D. C. Current-Driven Magnetization Reversal and Spin-Wave Excitations in Co /Cu /Co Pillars. *Phys. Rev. Lett.* **2000**, *84*, 3149−3152.

(2) Weisheit, M.; Fahler, S.; Marty, A.; Souche, Y.; Poinsignon, C.; Givord, D. Electric Field-Induced Modification of Magnetism in Thin-Film Ferromagnets. *Science* **2007**, *315*, 349−351.

(3) Beaurepaire, E.; Merle, J.-C.; Daunois, A.; Bigot, J.-Y. Ultrafast Spin Dynamics in Ferromagnetic Nickel. *Phys. Rev. Lett.* **1996**, *76*, 4250−4253.

(4) Němec, P.; Fiebig, M.; Kampfrath, T.; Kimel, A. V. Antiferromagnetic opto-spintronics. *Nat. Phys.* **2018**, *14*, 229−241.

(5) Cenker, J.; Sivakumar, S.; Xie, K.; Miller, A.; Thijssen, P.; Liu, Z.; Dismukes, A.; Fonseca, J.; Anderson, E.; Zhu, X.; Roy, X.; Xiao, D.; Chu, J.-H.; Cao, T.; Xu, X. Reversible strain-induced magnetic phase transition in a van der Waals magnet. *Nat. Nanotechnol.* **2022**, *17*, 256−261.

(6) Li, T.; Jiang, S.; Sivadas, N.; Wang, Z.; Xu, Y.; Weber, D.; Goldberger, J. E.; Watanabe, K.; Taniguchi, T.; Fennie, C. J.; Mak, K. F.; Shan, J. Pressure-controlled interlayer magnetism in atomically thin CrI_3. *Nat. Mater.* **2019**, *18*, 1303−1308.

(7) Song, T.; Fei, Z.; Yankowitz, M.; Lin, Z.; Jiang, Q.; Hwangbo, K.; Zhang, Q.; Sun, B.; Taniguchi, T.; Watanabe, K.; McGuire, M. A.; Graf, D.; Cao, T.; Chu, J. H.; Cobden, D. H.; Dean, C. R.; Xiao, D.; Xu, X. Switching 2D magnetic states via pressure tuning of layer stacking. *Nat. Mater.* **2019**, *18*, 1298−1302.

(8) Jiang, X.; Liu, Q.; Xing, J.; Liu, N.; Guo, Y.; Liu, Z.; Zhao, J. Recent progress on 2D magnets: Fundamental mechanism, structural design and modification. *Applied Physics Reviews* **2021**, *8*, 031305.

(9) Wang, Q. H.; Bedoya-Pinto, A.; Blei, M.; Dismukes, A. H.; Hamo, A.; Jenkins, S.; Koperski, M.; Liu, Y.; Sun, Q.-C.; Telford, E. J.; et al. The Magnetic Genome of Two-Dimensional van der Waals Materials. *ACS Nano* **2022**, *16*, 6960−7079.

(10) Zhong, D.; Seyler, K. L.; Linpeng, X.; Cheng, R.; Sivadas, N.; Huang, B.; Schmidgall, E.; Taniguchi, T.; Watanabe, K.; McGuire, M. A.; Yao, W.; Xiao, D.; Fu, K.-M. C.; Xu, X. Van der Waals engineering of ferromagnetic semiconductor heterostructures for spin and valleytronics. *Science Advances* **2017**, *3*, No. e1603113.

(11) Ciorciaro, L.; Kroner, M.; Watanabe, K.; Taniguchi, T.; Imamoglu, A. Observation of Magnetic Proximity Effect Using Resonant Optical Spectroscopy of an Electrically Tunable $MoSe_2$/$CrBr_3$ Heterostructure. *Phys. Rev. Lett.* **2020**, *124*, 197401.

(12) Huang, B.; Clark, G.; Navarro-Moratalla, E.; Klein, D. R.; Cheng, R.; Seyler, K. L.; Zhong, D.; Schmidgall, E.; McGuire, M. A.; Cobden, D. H.; Yao, W.; Xiao, D.; Jarillo-Herrero, P.; Xu, X. Layer-dependent ferromagnetism in a van der Waals crystal down to the monolayer limit. *Nature* **2017**, *546*, 270−273.

(13) Gong, C.; Li, L.; Li, Z.; Ji, H.; Stern, A.; Xia, Y.; Cao, T.; Bao, W.; Wang, C.; Wang, Y.; Qiu, Z. Q.; Cava, R. J.; Louie, S. G.; Xia, J.; Zhang, X. Discovery of intrinsic ferromagnetism in two-dimensional van der Waals crystals. *Nature* **2017**, *546*, 265−269.

(14) Mermin, N. D.; Wagner, H. Absence of Ferromagnetism or Antiferromagnetism in One- or Two-Dimensional Isotropic Heisenberg Models. *Phys. Rev. Lett.* **1966**, *17*, 1133−1136.

(15) Jenkins, S.; Rózsa, L.; Atxitia, U.; Evans, R. F. L.; Novoselov, K. S.; Santos, E. J. G. Breaking through the Mermin-Wagner limit in 2D van der Waals magnets. *Nat. Commun.* **2022**, *13*, 6917.

(16) Yankowitz, M.; Chen, S.; Polshyn, H.; Zhang, Y.; Watanabe, K.; Taniguchi, T.; Graf, D.; Young, A. F.; Dean, C. R. Tuning superconductivity in twisted bilayer graphene. *Science* **2019**, *363*, 1059−1064.

(17) Hsu, W.-T.; Quan, J.; Pan, C.-R.; Chen, P.-J.; Chou, M.-Y.; Chang, W.-H.; MacDonald, A. H.; Li, X.; Lin, J.-F.; Shih, C.-K. Quantitative determination of interlayer electronic coupling at various critical points in bilayer MoS_2. *Phys. Rev. B* **2022**, *106*, 125302.

(18) Xia, J.; Yan, J.; Wang, Z.; He, Y.; Gong, Y.; Chen, W.; Sum, T. C.; Liu, Z.; Ajayan, P. M.; Shen, Z. Strong coupling and pressure engineering in WSe_2-$MoSe_2$ heterobilayers. *Nat. Phys.* **2021**, *17*, 92−98.

(19) Pawbake, A.; Pelini, T.; Delhomme, A.; Romanin, D.; Vaclavkova, D.; Martinez, G.; Calandra, M.; Measson, M.-A.; Veis, M.; Potemski, M.; Orlita, M.; Faugeras, C. High-Pressure Tuning of Magnon-Polarons in the Layered Antiferromagnet $FePS_3$. *ACS Nano* **2022**, *16*, 12656−12665.

(20) Telford, E. J.; Dismukes, A. H.; Lee, K.; Cheng, M.; Wieteska, A.; Bartholomew, A. K.; Chen, Y.-S.; Xu, X.; Pasupathy, A. N.; Zhu, X.; Dean, C. R.; Roy, X. Layered Antiferromagnetism Induces Large Negative Magnetoresistance in the van der Waals Semiconductor CrSBr. *Adv. Mater.* **2020**, *32*, 2003240.

(21) Liu, W.; Guo, X.; Schwartz, J.; Xie, H.; Dhale, N. U.; Sung, S. H.; Kondusamy, A. L. N.; Wang, X.; Zhao, H.; Berman, D.; Hovden, R.; Zhao, L.; Lv, B. A Three-Stage Magnetic Phase Transition Revealed in Ultrahigh-Quality van der Waals Bulk Magnet CrSBr. *ACS Nano* **2022**, *16*, 15917−15926.

(22) Telford, E. J.; Dismukes, A. H.; Dudley, R. L.; Wiscons, R. A.; Lee, K.; Yu, J.; Shabani, S.; Scheie, A.; Watanabe, K.; Taniguchi, T.; Xiao, D.; Pasupathy, A. N.; Nuckolls, C.; Xiaoyang, Z.; Dean, C. R.; Roy, X. Hidden low-temperature magnetic order revealed through magnetotransport in monolayer CrSBr. *arXiv*, June 15, 2021, 2106.08471, ver. *1*. DOI: 10.48550/arXiv.2106.08471.

(23) López-Paz, S. A.; Guguchia, Z.; Pomjakushin, V. Y.; Witteveen, C.; Cervellino, A.; Luetkens, H.; Casati, N.; Morpurgo, A. F.; von Rohr, F. O. Dynamic magnetic crossover at the origin of the hidden-order in van der Waals antiferromagnet CrSBr. *Nat. Commun.* **2022**, *13*, 4745.

(24) Klein, J.; et al. Sensing the Local Magnetic Environment through Optically Active Defects in a Layered Magnetic Semiconductor. *ACS Nano* **2023**, *17*, 288−299.

(25) Pawbake, A.; Pelini, T.; Wilson, N. P.; Mosina, K.; Sofer, Z.; Heid, R.; Faugeras, C. Raman scattering signatures of strong spin-phonon coupling in the bulk magnetic van der Waals material CrSBr. *Phys. Rev. B* **2023**, *107*, 075421.

(26) Wilson, N. P.; Lee, K.; Cenker, J.; Xie, K.; Dismukes, A. H.; Telford, E. J.; Fonseca, J.; Sivakumar, S.; Dean, C.; Cao, T.; Roy, X.; Xu, X.; Zhu, X. Interlayer electronic coupling on demand in a 2D magnetic semiconductor. *Nat. Mater.* **2021**, *20*, 1657−1662.

(27) Long, F.; Mosina, K.; Hübner, R.; Sofer, Z.; Klein, J.; Prucnal, S.; Helm, M.; Dirnberger, F.; Zhou, S. Intrinsic magnetic properties of the layered antiferromagnet CrSBr. *arXiv*, September 9, 2023, 2309.04778, ver. *1*. DOI: 10.48550/arXiv.2309.04778.
(28) Avsar, A. Highly anisotropic van der Waals magnetism. *Nat. Mater.* **2022**, *21*, 731−733.
(29) Klein, J.; Pingault, B.; Florian, M.; Heißenbüttel, M. C.; Steinhoff, A.; Song, Z.; Torres, K.; Dirnberger, F.; Curtis, J. B.; Weile, M.; Penn, A.; Deilmann, T.; Dana, R.; Bushati, R.; Quan, J.; Luxa, J.; Sofer, Z.; Alù, A.; Menon, V. M.; Wurstbauer, U.; Rohlfing, M.; Narang, P.; Lončar, M.; Ross, F. M. The Bulk van der Waals Layered Magnet CrSBr is a Quasi-1D Material. *ACS Nano* **2023**, *17*, 5316−5328.
(30) Wu, F.; Gutiérrez-Lezama, I.; López-Paz, S. A.; Gibertini, M.; Watanabe, K.; Taniguchi, T.; von Rohr, F. O.; Ubrig, N.; Morpurgo, A. F. Quasi-1D Electronic Transport in a 2D Magnetic Semiconductor. *Adv. Mater.* **2022**, *34*, 2109759.
(31) Bae, Y. J.; et al. Exciton-coupled coherent magnons in a 2D semiconductor. *Nature* **2022**, *609*, 282−286.
(32) Cham, T. M. J.; Karimeddiny, S.; Dismukes, A. H.; Roy, X.; Ralph, D. C.; Luo, Y. K. Anisotropic Gigahertz Antiferromagnetic Resonances of the Easy-Axis van der Waals Antiferromagnet CrSBr. *Nano Lett.* **2022**, *22*, 6716−6723.
(33) Cho, C. W.; Pawbake, A.; Aubergier, N.; Barra, A. L.; Mosina, K.; Sofer, Z.; Zhitomirsky, M. E.; Faugeras, C.; Piot, B. A. Microscopic parameters of the van der Waals CrSBr antiferromagnet from microwave absorption experiments. *Phys. Rev. B* **2023**, *107*, 094403.
(34) Breslavetz, I.; Delhomme, A.; Pelini, T.; Pawbake, A.; Vaclavkova, D.; Orlita, M.; Potemski, M.; Measson, M.-A.; Faugeras, C. Spatially resolved optical spectroscopy in extreme environment of low temperature, high magnetic fields and high pressure. *Rev. Sci. Instrum.* **2021**, *92*, 123909.
(35) Dirnberger, F.; Quan, J.; Bushati, R.; Diederich, G. M.; Florian, M.; Klein, J.; Mosina, K.; Sofer, Z.; Xu, X.; Kamra, A.; García-Vidal, F. J.; Alù, A.; Menon, V. M. Magneto-optics in a van der Waals magnet tuned by self-hybridized polaritons. *Nature* **2023**, *620*, 533−537.
(36) Scheie, A.; Ziebel, M.; Chica, D. G.; Bae, Y. J.; Wang, X.; Kolesnikov, A. I.; Zhu, X.; Roy, X. Spin Waves and Magnetic Exchange Hamiltonian in CrSBr. *Advanced Science* **2022**, *9*, 2202467.
(37) Néel, L. Antiferromagnetism and Ferrimagnetism. *Proceedings of the Physical Society. Section A* **1952**, *65*, 869−885.
(38) Göser, O.; Paul, W.; Kahle, H. Magnetic properties of CrSBr. *J. Magn. Magn. Mater.* **1990**, *92*, 129−136.
(39) Telford, E. J.; Chica, D. G.; Ziebel, M. E.; Xie, K.; Manganaro, N. S.; Huang, C.-Y.; Cox, J.; Dismukes, A. H.; Zhu, X.; Walsh, J. P. S.; Cao, T.; Dean, C. R.; Roy, X. Designing Magnetic Properties in CrSBr through Hydrostatic Pressure and Ligand Substitution. *Advanced Physics Research* **2023**, 2300036.

https://doi.org/10.1021/acs.nanolett.3c03216
Nano Lett. 2023, 23, 9587−9593